

Compact and integrated 2-D photonic crystal super-prism filter-device for wavelength demultiplexing applications

A. S. Jugessur, A. Bakhtazad, A. G. Kirk

*Photonic Systems Group, Department of Electrical and Computer Engineering, McGill University
3480, University Street, Montreal, Canada, H3A 2A7
aju@photonics.ece.mcgill.ca*

L. Wu

*Laboratory for Photonic Information Technology, School for Information and Optoelectronic Science and Engineering, South China Normal University, Guangzhou China 510631
ljwn@scnu.edu.cn*

T. F. Krauss

*Ultrafast Photonics Collaboration, School of Physics and Astronomy, University of St-Andrews
St-Andrews, KY16 9SS, Scotland, U.K*

R. M. De La Rue

*Optoelectronics Research Group, Department of Electrical and Electronic Engineering, University of Glasgow
Oakfield Avenue, Glasgow, G12 8LT, Scotland, U.K*

Abstract: A two-dimensional photonic crystal (PhC) super-prism integrated with one-dimensional photonic crystal microcavity filters has been designed using the plane wave expansion (PWE) and 2-D Finite Difference Time Domain (FDTD) methods based on Silicon-on-Insulator (SOI) technology. The super-prism operates as a coarse spatial filter with an average response bandwidth of 60 nm, while the 1-D PhC microcavity filters operate as narrow band-pass transmission filters with an average filter response line-width of 10 nm. This work demonstrates the simultaneous operation of two photonic devices for de-multiplexing applications on a single platform that could be useful in future Photonic Crystal Integrated Circuits (PCICs).

© 2006 Optical Society of America

OCIS codes: (999.9999) Photonic crystals; (230.3120) Integrated optics devices; (250.5300) Photonic integrated circuits

References and links

1. S. Y. Lin, V. M. Hietala, L. Wang and E. D. Jones, "Highly dispersive photonic band-gap prism," *Opt. Lett.* **21**, 1771-1773 (1996)
2. H. Hosaka, T. Kawashima, A. Tomita, M. Notomi, T. Tamamura, T. Sato and S. Kawakami, "Superprism phenomena in photonic crystals," *Phys. Rev. B* **58**, R10096-R10099 (1998)
3. B. Momeni and A. Adibi, "Optimization of photonic crystal demultiplexers based on the superprism effect," *Appl. Phys. B* **77**, 555-560 (2003)
4. L. Wu, M. Mazilu, J. -F. Gallet and T. F. Krauss, "Square lattice photonic-crystal collimator," *Photonics and Nanostructures – Fundamentals and Applications*, 31-36 (2003)
5. L. Wu, M. Mazilu and T. F. Krauss, "Beam Steering in Planar-Photonic Crystals: From Superprism to Supercollimator," *J. Lightwave Technol.* **21**, 561-566 (2003)

6. L. Wu, M. Mazilu, T. Karle and T. F. Krauss, "Superprism Phenomena in Planar Photonic Crystals," *IEEE J. Quantum Opt.* **38**, 915-918 (2002)
 7. L. Wu, M. Mazilu, J.-F. Gallet, T. F. Krauss, A. Jugessur and R. M. De La Rue, "Planar photonic crystal polarization splitter," *Opt. Lett.* **29**, 1620-1622 (2004)
 8. T. Matsumoto and T. Baba, "Photonic Crystal k-Vector Superprism," *J. Lightwave Technol.* **22**, 917-922 (2004)
 9. B. Song, S. Noda and T. Asano, "Photonic Devices Based on In-plane Hetero Photonic Crystals," *Science* **300**, 1537 (2003)
 10. A. Sharkawy, S. Shi and D. W. Prather, "Multichannel wavelength division multiplexing with photonic crystals," *Appl. Opt.* **40**, 2247-2252 (2001)
 11. L. Wu, M. Mazilu, J.-F. Gallet and T. F. Krauss, "Dual lattice photonic-crystal beam splitters," *Appl. Phys Lett.* **86**, 211106 (2005)
 12. A. S. Jugessur, P. Pottier and R. M. De La Rue, "One dimensional periodic photonic crystals microcavity filters with transition mode-matching features, embedded in ridge waveguides," *Electron. Lett.* **39**, 367-368 (2003)
 13. A. S. Jugessur, P. Pottier, and R. M. De La Rue, "Engineering the filter response of photonic crystals microcavity filters," *Opt. Express* **12**, 1304-1312 (2004)
 14. T. Baba and D. Ohsaki, "Interfaces of photonic crystals for high efficiency light transmission," *Jpn. J. Appl. Phys.* **40**, 5920-5924 (2001)
 15. J. Witzens, M. Hochberg, T. Baehr-Jones and A. Scherer, "Mode-matching interface for efficient coupling of light into planar photonic crystals," *Phys. Rev. E* **69**, 046609-1-12 (2004)
-

1. Introduction

Photonic crystals have stirred the engineering imagination of many scientists since they offer many ways to control the propagation of light. In some of the reported applications, the photonic band gap, where optical propagation is prohibited at certain frequencies, has been exploited, for example, in the confinement of light in photonic crystal channel waveguides and photon confinement in cavity-based devices. However, there are applications which rely on the propagation of light within the photonic crystal structures – and these are based on the anomalous dispersion behaviour near the photonic band-edges. This phenomenon is widely known as the super-prism effect and has recently been the subject of intensive study. Previous studies [1,2,3] focused on the theoretical analysis of this type of device and some proofs of concept demonstrated by experimental results [4,5,6], where the measured spectra clearly showed beam-steering and collimation at different wavelengths. Also, the splitting of light into different polarizations has been demonstrated experimentally in 2-D PhC super-prisms [7]. Nevertheless, the experimental spectra obtained so far show transmission peaks with broad line-widths. The main limitation that restricts the separation of wavelengths inside a PhC structure is the cross-talk caused by the divergence of the input beam. In order to avoid the mixing of adjacent channels, a very small divergence of the input beam is needed, which results in a relatively large structure [8]. The present compact and integrated 2D-PhC super-prism filter-device addresses these issues. In this new device, the 2-D PhC super-prism pre-selects the wavelength and the 1-D PhC filters integrated with the super-prism refine the spectral response (see Fig. 1). In other words, the super-prism operates as a coarse demultiplexing device while the 1-D PhC microcavity filters operate as narrow band-pass transmission filters. It is worth noting that such simple demultiplexing could also be carried out by a combination of star-couplers and band-pass filters. Nevertheless, for that combination, the input power is almost equally distributed at the output channels, whereas in our present device the power is steered towards the desired channels. Moreover, for an equivalent demultiplexing capability as the present device, star couplers are longer ($>100\ \mu\text{m}$) and losses are comparable to our device. There are also other 2-D photonic crystal demultiplexers based on a different approach which is a multichannel wavelength add-drop functionality [9,10], where the microcavities are embedded in the lattice.

In the present design, both the input and output interfaces are kept normal to the incident beam to guarantee that the phase velocity remains normal to the interfaces everywhere. Hence, all the output waveguides are placed in parallel for maximum output light coupling. This integration scheme combines the operation of two photonic devices on the same platform and is therefore a useful demonstration of the Photonic Crystal Integrated Circuit (PCIC) approach.

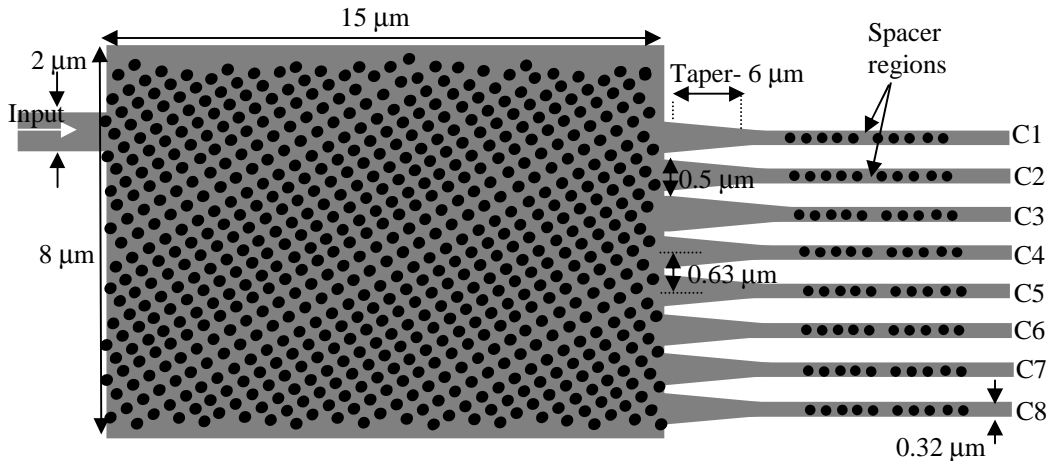


Fig. 1. Schematic (not to scale) of the combined photonic system of a 2-D PhC super-prism integrated with 1-D PhC filters.

2. Design of the 2-D photonic crystal super-prism using Plane Wave Expansion (PWE) and 2-D Finite Domain Time Difference (FDTD) methods

The platform chosen for this work is Silicon-on-Insulator (SOI) planar waveguide technology with a top guiding core thickness of 260 nm. A square lattice is chosen for the super-prism because of its greater asymmetry in the first band, resulting in larger angular dispersion compared with a hexagonal-lattice PhC structure [11]. The light is polarised with its E-field parallel to the axes of the air holes (corresponding to a TM-like mode), but a similar case can be constructed for TE-like polarisation. The lattice constant and the hole diameter were chosen to provide a wide wavelength span (1310 -1470 nm) at the band-edge of the first band. The lattice parameters which result in the desired wavelength range of operation were a period of 260 nm and hole diameter of 140 nm.

2.1 An equivalent 2-D model using PWE

Ideally, full 3-D modelling would be used to give a better evaluation of the behaviour of the device. However, it is computationally intensive and time-consuming to simulate the complete three-dimensional structure. By the same token, an equivalent 2-D model has to be developed. Effective index method has been used already [5,8] to get to a 2-D model but the assumption made has no physical basis, and it does not follow the band diagram obtained using the 3-D model. Here, a new method is introduced which has not been reported elsewhere to our knowledge. An equivalent 2-D model could be obtained by matching the band-edge of the wave-vector diagram of the 3-D model to an equivalent 2-D model with appropriate effective refractive indices. In others words, the refractive indices of the slab and air hole are modified until the 2-D band-edge effective refractive indices ($n_x = k_x/k_0$) matches as closely as possible (in a root mean square sense) to its 3-D counterpart in the desired wavelength range of interest (1310-1470 nm). More precisely, the following error function, Eq. (1), has been minimized versus n_{slab} and n_{hole} .

$$E(n_{\text{slab}}, n_{\text{hole}}) = \int_{\lambda_1}^{\lambda_2} [n_x^{2\text{-D}}(\lambda, n_{\text{slab}}, n_{\text{hole}}) - n_x^{3\text{-D}}(\lambda)]^2 d\lambda \quad (1)$$

where $\lambda_1, \lambda_2 = 1310$ and 1470 nm, respectively,

$$\begin{aligned} n_x^{2\text{-D}}(\lambda, n_{\text{slab}}, n_{\text{hole}}) &= \text{effective index at band-edge of 2-D model} \\ n_x^{3\text{-D}}(\lambda) &= \text{effective index at band-edge of 3-D model} \end{aligned}$$

The best fit 2-D effective refractive indices obtained are:

$$n_{\text{slab}} = 2.85 \text{ and } n_{\text{hole}} = 1.94$$

The map of the band-edge versus wavelength is plotted in Fig. 2, showing the results of 3-D modelling and the corresponding 2-D best fit. Comparison of the band diagrams of the 3-D model and the equivalent 2-D best-fit shows that, while the band edges in the 2-D best fit case are very close to the 3-D band edge (as can be seen from Fig. 2), the band shapes do not follow the same trends. As a result, some discrepancy between results based on the wave diagrams of the 3-D modelling and the equivalent 2-D modelling should be expected. This limitation highlights the desirability of using 3-D FDTD modelling.

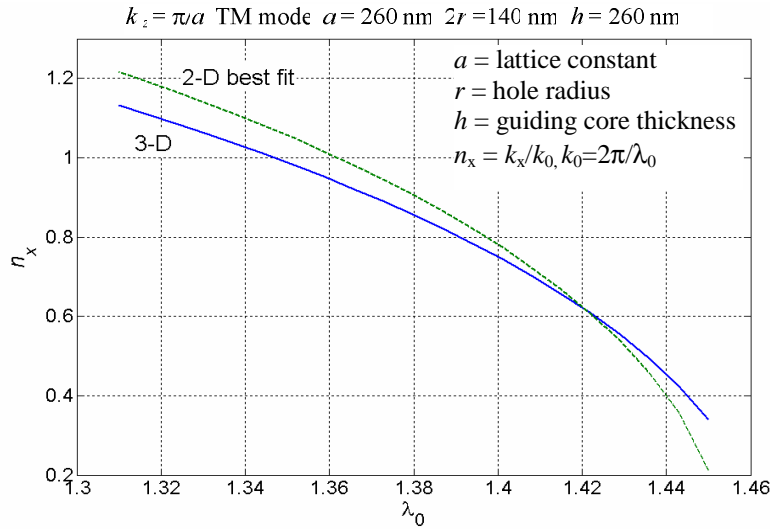


Fig. 2. The band edge map of the slab 2-D photonic crystal based on 3-D modelling and the best fit 2-D model.

The slab effective index can be taken as the refractive index of the free space region at the desired wavelength and specified polarization. In our case it is $n_{\text{free}} = 3.0113$.

Band diagrams can be obtained using plane-wave expansion (PWE) method, but, in order to apply the 3-D PWE method to a slab photonic crystal, an artificial periodicity needs to be applied in the direction normal to the super-prism slab surface. With the present high index contrast material, an imaginary unit cell four times wider than the super-prism slab is considered sufficient. In order to achieve a sufficiently accurate wave vector diagram (Section

2.2), the structure is discretised using a 8 nm mesh size while averaging the refractive index over a finer mesh that is eight times smaller. The entire first Brillion zone was then scanned through 4×10^4 points for more accurate results. It is worth noting that the equivalent 2-D model with slab and hole refractive indices of 2.85 and 1.94, respectively have been used in the 2-D FDTD modelling in Section 2.3.

2.2 Modelling results from the Plane Wave Expansion Method

The refraction and the beam direction are easily obtained using the wave-vector diagram obtained from the equi-frequency contours of the band diagram which is only part of the complete band diagram [1,2,6] of a 2-D photonic crystal structure.

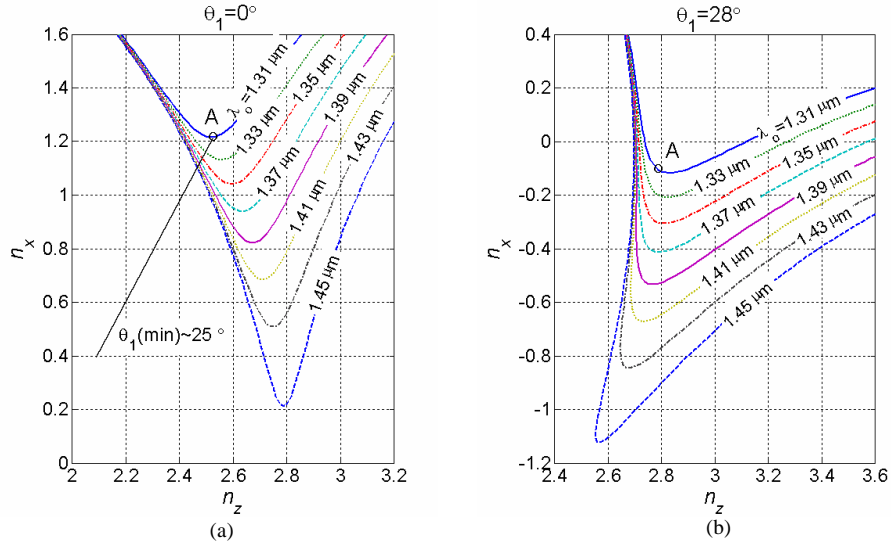


Fig. 3. Normalized equi-frequency band diagram near the band edge at the wavelength of interest ($n_z \equiv k_z/k_0$ and $n_x \equiv k_x/k_0$) (a) without rotation (b) with a rotation of 28° .

For the sake of simplicity, in this particular design, the input waveguide is normal to the input interface. As a result, the tangential component of the input wave vector is zero and unchanged through the input interface. From Fig. 3(a), it can be seen that to avoid the band-gap, the bulk PhC structure has to be rotated by at least 25° (refer to A), i.e.,

$$\theta_1(\text{min}) = \tan^{-1}\left(\frac{1.2}{2.51}\right) \approx 25^\circ$$

Assuming a margin of 10% for having more robust device, an angle of rotation of

$$\theta_1 = \tan^{-1}\left(\frac{1.2 \times 1.1}{2.52}\right) \approx 28^\circ$$

seemed reasonable and was implemented in our present design. Figure 3(b) shows the rotated band diagram and the new location of point A.

Since the tangential component of the input wave vector is zero, the tangential component of the wave vector is also zero at the output interface, provided the output interface is kept parallel to the input interface. Consequently, the output waveguides need to be aligned normal to the output interface in order to be directed in the direction of transmitted

wave. Figure 4 shows the steering angle for the incident plane wave (the angle between the incident wave and transmitted wave) versus wavelength - which is always negative since the direction of the gradient of the rotated wave vector diagram near the band-edge of the first band of a square lattice always points downward.

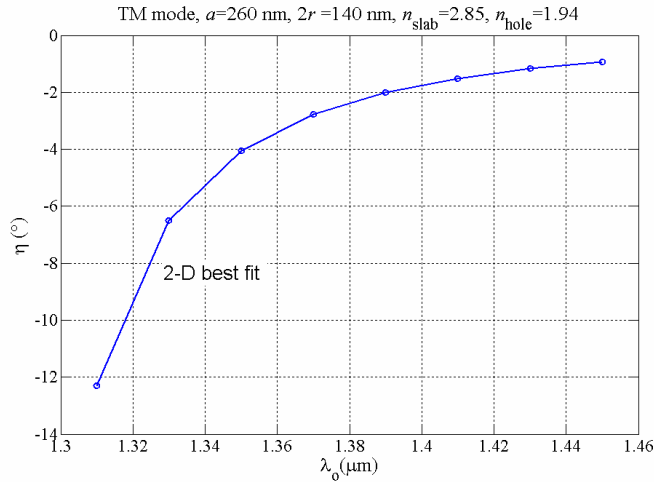


Fig. 4. Steering angle versus wavelength based on 2-D best fit model when the PhC structure is rotated by 28°.

As can be seen, the steering angle variation with wavelength is nonlinear; the dispersion is high at the beginning of the band and decreases away from the band-edge.

2.3 Modelling using 2-D FDTD based computation

The beam deviation angle (angle between the transmission and input beam, i.e. steering angle for finite beam widths) versus the input width at $\lambda_0 = 1.31 \mu\text{m}$ is shown in Fig. 5 (computed using the 2-D FDTD). As can be seen, for input widths greater than $3 \mu\text{m}$, the beam deviation angle increases with the input waveguide width and approaches the steering angle obtained by PWE shown in Fig. 4. This can be interpreted as being in agreement with the fact that the angular spectrum of the Gaussian beam decreases as the spatial beam-width increases. Therefore, a larger region of the wave vector diagram interacts with the angular spectrum of the input beam when the beam-width is small. Then, with the high dispersion non-uniformity (as observed in Fig. 4), it is plausible that the beam deviation angle reduces with decreasing input beam-width. The beam deviation angle increases again as the input waveguide width decreases below $3 \mu\text{m}$. This could be due to the fact that, the Gaussian beam approximation for propagation in the photonic crystal becomes less valid in this region.

Further investigation is needed to explain the occurrence of the smallest beam deviation angle at an input width of $3 \mu\text{m}$. In this particular design, an input waveguide width of $2 \mu\text{m}$ was chosen, which resulted in a beam deviation angle of approximately 10.2 degrees. This input width was considered appropriate because it allowed sufficient light to penetrate the PhC structure and gave an acceptable level of spectrum overlapping at the output interface.

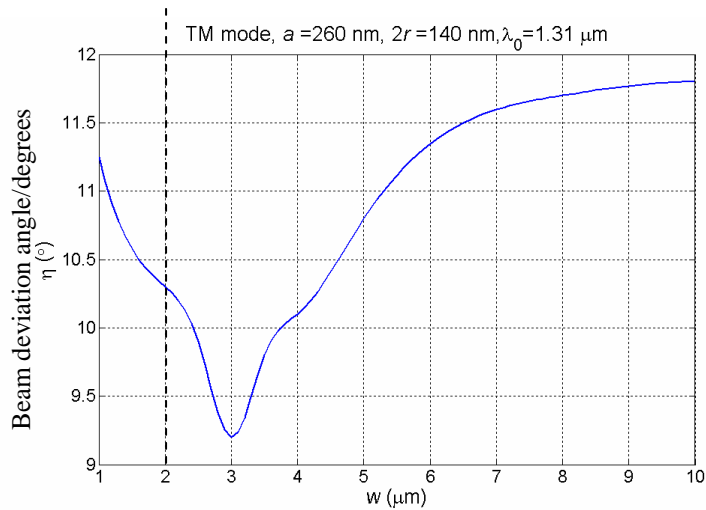


Fig. 5. The beam deviation angle versus input waveguide width, using 2-D FDTD modelling, based on a 2-D best fit.

The transmission spectra (obtained by 2-D FDTD) of the super-prism device for the eight output channel waveguides are shown in Fig. 6.

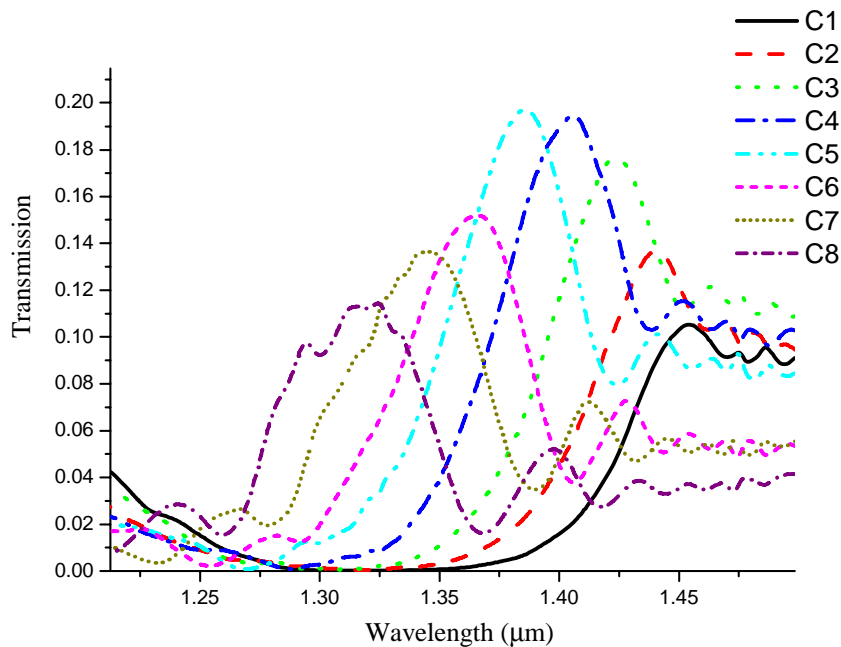


Fig. 6. Transmission spectra of the 2-D PhC super-prism at the output waveguides.

A pulsed broadband source in the wavelength range 1300-1470 nm was used to excite the input waveguide in the TM polarization. The device was discretized with a mesh size of 10 nm. The schematic layout of the super-prism is as shown in Fig. 1, which shows 8 output waveguides of 0.5 μm width tapered down adiabatically to 0.3 μm for single-mode guidance. The effective indices of 2-D best fit obtained in the previous Section 2.1 have been used. Frequency Domain Power monitors were used to collect the data at each output channel

waveguide. Perfectly matched layer boundaries were chosen to allow the radiation to leave the boundary without reflecting back inside. As can be seen from the transmission spectra in Fig. 6, the bandwidths of the transmission peaks are broad (> 50 nm) and overlapping. The latter observation is due to the fact that the channels are closely packed and each channel is receiving only a section of the spectrum. The spectral resolution of the super-prism is approximately 20 nm. An angular dispersion of $0.4^\circ/\text{nm}$ was achieved with this design. Higher dispersion could be achieved if wavelength range was compromised, but it is not the main objective of the present work. This method of collecting the output light is different from other designs where wider channels (placed radially) and larger PhC areas have been used to ensure a higher spatial wavelength separation [4,5,6]. In our design, the transmission peaks from each channel overlap - which is not ideal for many applications. Nevertheless, in the present configuration, the super-prism with the specific output waveguide sizes chosen pre-selects the wavelength (giving a coarse filtering action). The fine filtering step is carried out with the 1-D PhC filters (see Fig. 1) embedded in the channel output waveguides. The crucial role of the filters is then to select a specific wavelength with a narrower spectral line-width and clean up the spectrum.

3. Design of 1-D PhC filters

The 1-D PhC filters have been designed to give a band-gap for TM polarised light in the range 1190 to 1600 nm. The hole sizes and periods of each individual filter for each channel have been numerically simulated independently using 2-D FDTD computation to cover specifically the entire wavelength span of the transmission output of the super-prism. It is important to design filters that have band gap ranges that fully cover the broad line-width of the super-prism spectral responses. A phase-shift is then introduced in the array of holes to give a narrow transmission band around the desired peak wavelength. It is worth noting that modelling and experimental work [12,13] on 1-D PhC filters have been carried out previously. Since the 1-D PhC filters have been designed for implementation on an SOI platform, an effective index of 3.0113 was used in the 2-D FDTD simulation. The stop-band range could be varied by adjusting the PhC hole size and periodicity. The parameters of each filter were carefully chosen so that the desired transmission resonance was spectrally located in the middle of the stop-band. The table below shows the parameters of each 1-D PhC filter at each peak wavelength.

Table 1. Parameters of 1-D PhC filters designed for specific wavelengths

Filter No.	Resonance Wavelength (nm)	a, period (nm)	d, diameter (nm)	Optical cavity length (nm)
1	1455	325	180	470
2	1440	330	200	470
3	1423	330	225	485
4	1406	330	245	471
5	1385	330	245	482
6	1365	330	245	465
7	1344	315	245	478
8	1324	315	245	460

Figure 7 shows a typical transmission spectrum of one of the PhC filters with a transmission stop-band ranging from approximately 1190 to 1600 nm, with the transmission peak spectrally positioned at 1360 nm. The inset shows a schematic of the device. As shown in the inset of Fig. 7, the 1-D PhC filters consist of seven PhC holes on each side of the microcavity, leading to sufficiently high Q-factors (~ 250) for the filtering function.

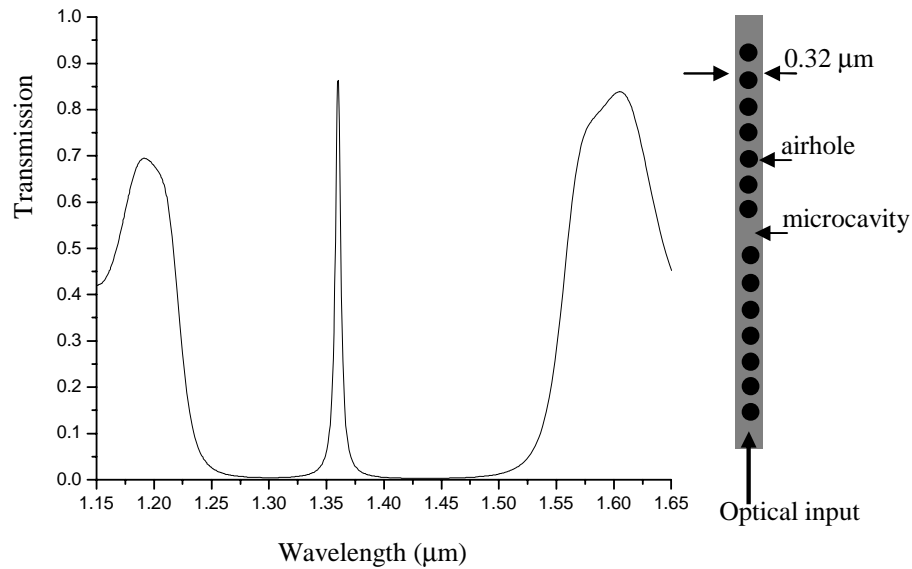


Fig. 7. Transmission band gap of a 1-D PhC filter showing a peak resonance at 1360 nm with a schematic of the device in the inset.

4. Combined photonic system of 2-D PhC super-prism and 1-D PhC filters

The combined photonic system consisting of the 2-D PhC super-prism with 1-D PhC filters, including the short waveguide tapers, is shown schematically in Fig. 1. The tapers (from 0.5 μm tapered down to 0.32 μm) were designed using 2-D FDTD simulation. A taper angle of 0.8° was chosen to ensure an adiabatic modal conversion from multimode to single mode over a taper length of approximately 6 μm . As shown in Fig. 1, eight different versions of the 1-D PhC filter were placed with one at each output channel waveguide of the super-prism. Since the 2-D FDTD modelling of this combined photonic system (2-D PhC super-prism, 1-D PhC filters and tapers) becomes cumbersome, the transmission coefficient from each super-prism output channel was multiplied by the transmission coefficient of the corresponding 1-D PhC filter. This approach is valid since the reflection from the 1-D PhC filters is small (0.3-0.6 dB) and yields very little back-reflection from the 1-D PhC filters towards the super-prism. Figure 8 shows the transmission spectra for each of the 1-D PhC filters embedded in the eight channels – and clearly shows the fine wavelength selection obtained for eight particular wavelengths, as well as the ‘clean up’ of the signal response from the super-prism.

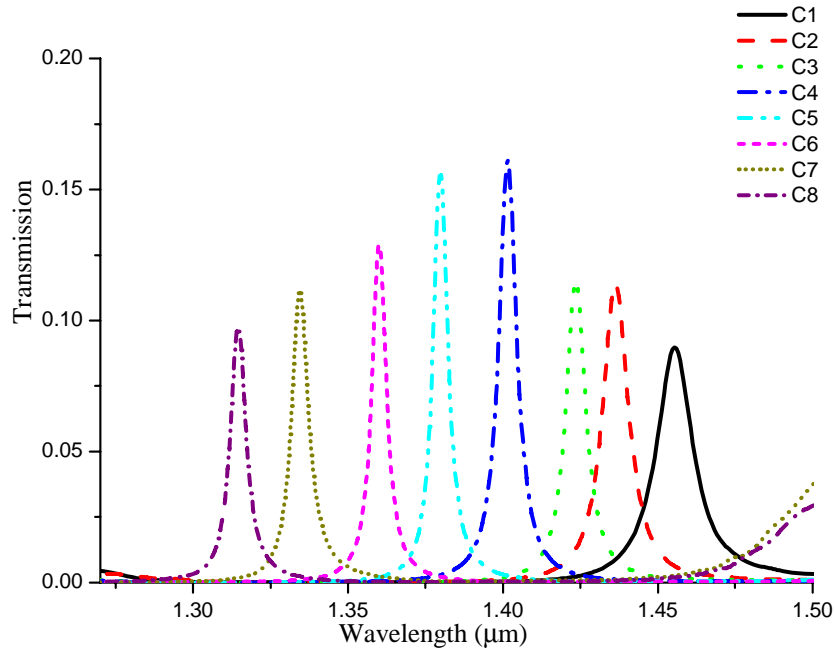


Fig. 8. Transmission spectra of the combined photonic system of super-prism and filter.

The average line-width of the filters is 9 ± 4 nm, which is much narrower than that of the super-prism. The worst 3-dB cross-talk occurred in channel 1 and was approximately -5.0 dB. The maximum optical loss was obtained from channel 1, with a value of approximately 10.5 dB (see Fig. 8). The maximum optical loss through the super-prism structure only is approximately 9.5 dB (see Fig. 6). The 1-D PhC filters contribute to a maximum theoretical optical loss of about 1 dB. The major sources of losses come from the PhC region to waveguide interfaces (at the waveguide-superprism interface near the input and output regions) and the out-of-plane scattering loss which is not taken into account in the 2D FDTD computation. The transition regions at the tapers also introduce some losses. The losses could be reduced by adding mode-matching features [12,14,15] at the PhC-waveguide interfaces. Particularly, previous work [15] has shown that the insertion efficiency at PhC-waveguide interfaces can be significantly increased by imposing multilayered grating structures at those transition zones. It is worth noting that this device is sensitive to fabrication errors – a 5-10 % change in the 1D PhC filters hole size could shift the spectral position of the peak transmission wavelength by 5-10 nm [12]. Nevertheless, since the bandwidths of the superprism spectral responses are broad, the fabrication tolerance of the 1D PhC filters is not that strict. The filter responses have a Lorentzian profile, which is not ideal for many applications. By the same token, the responses could possibly be tailored to a quasi-rectangular and steeper-edge responses [13], to reduce channel cross-talk further and hence, more suitable for de-multiplexing applications. One of the future directions of this work could be to carry out the demultiplexing operation with one lattice type and the more refined wavelength selectivity with microcavities embedded on a different lattice type – a dual photonic crystal lattice, leading to a more compact device.

5. Conclusions

A compact and integrated photonic crystal super-prism-filter device with a spectral resolution of 20 nm and a footprint of less than $30 \times 8 \mu\text{m}$ has been designed using the Plane Wave Expansion and 2-D FDTD methods. This device resolves the challenge of fine wavelength selection and low crosstalk against small size in a photonic crystal superprism that has been discussed by several authors [1,6,8]. The 2-D PhC super-prism pre-selects the wavelength and the 1-D PhC filters carry out refined wavelength selection. This combination has a broader spectral bandwidth than previously demonstrated superprisms, yet features good spectral selectivity and low crosstalk, which makes it suitable for Coarse Wavelength Division Multiplexing (CWDM) applications. The combination of multiple photonic devices is a necessary stepping stone towards the realisation of larger scale Photonic Crystal Integrated Circuits (PCICs).

Acknowledgments

This work was supported by the Canadian National Science and Engineering Research Council (NSERC) under the strategic research networks program (Agile All-Photonic Networks) and by the Government of Quebec under the Valorization Recherche Quebec program (NanoQuebec). The support of the EPSRC (UK) through the Ultrafast Photonics Collaboration (UPC) is also acknowledged